Characterization of precipitation product errors across the United States using multiplicative triple collocation

Citation: Alemohammad, S. H., K. A. McColl, A. G. Konings, D. Entekhabi, and A. Stoffelen. "Characterization of Precipitation Product Errors Across the United States Using Multiplicative Triple Collocation." Hydrology and Earth System Sciences 19, no. 8 (2015): 3489–3503.

As Published: http://dx.doi.org/10.5194/hess-19-3489-2015

Publisher: Copernicus GmbH

Persistent URL: http://hdl.handle.net/1721.1/99663

Version: Final published version: final published article, as it appeared in a journal, conference proceedings, or other formally published context

Hydrol. Earth Syst. Sci., 19, 3489–3503, 2015
www.hydrol-earth-syst-sci.net/19/3489/2015/
doi:10.5194/hess-19-3489-2015

Hydrology and Earth System Sciences
Open Access

Characterization of precipitation product errors across the United States using multiplicative triple collocation

S. H. Alemohammad[1], K. A. McColl[1], A. G. Konings[1], D. Entekhabi[1], and A. Stoffelen[2]

[1]Department of Civil and Environmental Engineering, Massachusetts Institute of Technology, Cambridge, MA, USA
[2]Koninklijk Nederlands Meteorologisch Instituut (KNMI), R&D Satellite Observations, De Bilt, the Netherlands

Correspondence to: S. H. Alemohammad (hamed_al@mit.edu)

Received: 19 January 2015 – Published in Hydrol. Earth Syst. Sci. Discuss.: 27 February 2015
Revised: 8 July 2015 – Accepted: 27 July 2015 – Published: 10 August 2015

Abstract. Validation of precipitation estimates from various products is a challenging problem, since the true precipitation is unknown. However, with the increased availability of precipitation estimates from a wide range of instruments (satellite, ground-based radar, and gauge), it is now possible to apply the triple collocation (TC) technique to characterize the uncertainties in each of the products. Classical TC takes advantage of three collocated data products of the same variable and estimates the mean squared error of each, without requiring knowledge of the truth. In this study, triplets among NEXRAD-IV, TRMM 3B42RT, GPCP 1DD, and GPI products are used to quantify the associated spatial error characteristics across a central part of the continental US. Data are aggregated to biweekly accumulations from January 2002 through April 2014 across a $2^\circ \times 2^\circ$ spatial grid. This is the first study of its kind to explore precipitation estimation errors using TC across the US. A multiplicative (logarithmic) error model is incorporated in the original TC formulation to relate the precipitation estimates to the unknown truth. For precipitation application, this is more realistic than the additive error model used in the original TC derivations, which is generally appropriate for existing applications such as in the case of wind vector components and soil moisture comparisons. This study provides error estimates of the precipitation products that can be incorporated into hydrological and meteorological models, especially those used in data assimilation. Physical interpretations of the error fields (related to topography, climate, etc.) are explored. The methodology presented in this study could be used to quantify the uncertainties associated with precipitation estimates from each of the constellations of GPM satellites. Such quantification is prerequisite to optimally merging these estimates.

1 Introduction

Precipitation is one of the main drivers of the water cycle; therefore, accurate precipitation estimates are necessary for studying land–atmosphere interactions as well as linkages between the water, energy, and carbon cycles. Surface precipitation is also a principal driver of hydrologic models with a wide range of applications. A wide suite of instruments (in situ and remote sensing) monitor precipitation incident at the Earth's surface. Specifically, there has been a great effort during the last 2 decades to use microwave radar and radiometer instruments on board low-earth-orbit satellites to accurately estimate precipitation over large areas. These estimates, when combined with infrared-based cloud-top temperature observations from geostationary satellites, provide high spatial and temporal resolution precipitation estimates that are appropriate for hydrological and climatological studies.

However, precipitation estimation is inevitably subject to error. The errors are caused by different factors depending on the measurement instrument. For gauge measurements, the sparse distribution of gauges, environmental conditions such as wind and evaporation, and topography contribute to the errors. For ground-based radars, beam blockages in mountainous regions, the empirical backscatter–rain rate relationship (and the simplifications embedded in their functional form), and clutter are among the sources of error. Lastly, for satellite retrievals (both radiometer and radar), assumptions about the surface emissivity, neglecting evaporation below clouds, and empirical relationships are the driving factors of error.

The new Global Precipitation Measurement (GPM) mission aims to integrate precipitation estimates from a constellation of satellites to provide high spatial and temporal resolution estimates of precipitation over the Earth (Hou et al., 2013). However, successful data integration requires that the errors in each estimate are known. Since the truth is not known, only indirect methods are generally developed to estimate errors.

Several studies investigate and model the uncertainties in remotely-sensed precipitation estimates; however, they all depend on assuming the ground-based (gauge and/or radar) observations or models representing the zero-error precipitation (Krajewski et al. (2000); McCollum et al. (2002); Ebert et al. (2007); Su et al. (2008); Sapiano and Arkin (2009); Tian et al. (2009); Vila et al. (2009); Anagnostou et al. (2010); Stampoulis and Anagnostou (2012); Habib et al. (2012); Kirstetter et al. (2012, 2013); Chen et al. (2013); Alemohammad et al. (2014); Maggioni et al. (2014); Seyyedi (2014); Tang et al. (2014); Salio et al. (2015); Prat and Nelson (2015); Alemohammad et al. (2015); Gebregiorgis and Hossain (2015); among others).

Triple collocation (TC) provides a platform for quantifying the root mean square error (RMSE) in three or more products that estimate the same geophysical variable. Developed by Stoffelen (1998), TC takes advantage of at least three spatially and temporally collocated measurements of the variable of interest to solve a system of equations and estimate the error variance of each of the measurements. To make this system of equations determined, some assumptions are built into the technique including zero-error cross covariance between different products and zero covariance between errors and truth.

While TC has been used extensively to estimate errors in soil moisture products (Miralles et al., 2010; Dorigo et al., 2010; Parinussa et al., 2011; Anderson et al., 2012; Draper et al., 2013), it has also been successfully applied to other geophysical variables such as ocean wind speed and wave height (Stoffelen, 1998; Janssen et al., 2007; Portabella and Stoffelen, 2009), leaf area index (LAI) (Fang et al., 2012), fraction of absorbed photosynthetically active radiation (FAPAR) (D'Odorico et al., 2014), sea-ice thickness (Scott et al., 2014), atmospheric columnar integrated water vapor (Cimini et al., 2012; Thao et al., 2014), sea surface salinity (Ratheesh et al., 2013), and land water storage (van Dijk et al., 2014).

Roebeling et al. (2012) apply the TC technique to precipitation products for the first time and estimate errors for three precipitation products across Europe. The results show that a gridded gauge product and satellite retrievals (microwave) have TC errors less than 1.0 mm day^{-1} while the European weather radar estimates have errors up to 18 mm day^{-1} in some mountainous regions.

New variants of TC are introduced with wider applications in recent years. McColl et al. (2014) introduce the extended TC (ETC) that can be used to easily estimate the correlation coefficient between each of the triplets and the unknown truth as well as their RMSEs. ETC is mathematically equivalent to the original TC; however, the ease of calculating the correlation coefficients in ETC provides a different perspective on the performance of each product.

Su et al. (2014) introduce an implementation of instrument variables to reduce the minimum number of products necessary for TC analysis to two. In this framework, the lagged version of one of the two products is used as the third product to conduct the TC analysis (lagged-TC). If the lagged product is sampled at time intervals shorter than the temporal correlation length of the variable of interest, this approach can provide RMSE estimates of two collocated products.

In this study, we estimate the spatial RMSE between triplets of precipitation products across a central part of the US. Unlike Roebeling et al. (2012), we introduce a new logarithmic (multiplicative) error model that is more realistic for precipitation estimates. Moreover, the ETC approach is used in this study to estimate the correlation coefficients for each of the products.

Yilmaz and Crow (2014) present an extensive evaluation of the TC assumptions when applied to soil moisture products. We take a similar approach here, and use rain gauge data to validate the error estimates from TC analysis in a subset of pixels of the study domain. These pixels (located in the state of Oklahoma) have a dense network of rain gauges with a high quality data processing system that enables us to do this evaluation. The results of this evaluation provide a better understanding of the errors in precipitation products estimated by TC.

This paper is organized as following: Sect. 2 introduces the multiplicative TC analysis. Section 3 reviews the products used in this study. Section 4 presents the results of TC error estimates. Section 5 evaluates the assumptions of TC analysis using gauge data and Sect. 6 discusses the results and conclusions.

2 Triple collocation formulation

In this section, we review the TC formulation and introduce the multiplicative error model. In the multiplicative error model for precipitation, the true precipitation is related to the estimation as

$$\mathbf{R}_i = a_i \mathbf{T}^{\beta_i} e^{\epsilon_i}, \tag{1}$$

in which $\mathbf{R}_i$ is the precipitation intensity estimate from product i, $\mathbf{T}$ is the true precipitation intensity, a_i is the multiplicative error, β_i is the deformation error, and ϵ_i is the residual (random) error. The multiplicative error model is used in several studies to investigate the errors associated with precipitation estimates (Hossain and Anagnostou, 2006; Ciach et al., 2007; Villarini et al., 2009; Tian et al., 2013). It is generally concluded that the multiplicative model is more appropriate for quantifying errors in precipitation estimates. Moreover, Tian et al. (2013) present a comparison between the linear

and multiplicative error models applied to daily precipitation estimates across the US. They show that the multiplicative model has a better prediction skill and it is applicable to the variable and wide range of daily precipitation values. We also evaluated the joint probability density functions (PDF) of pairs of products to check their spread across different values of precipitation. Results show that PDFs generated from the multiplicative model have better spread compared to the additive model. Therefore, we concluded that for biweekly data it is better to assume the multiplicative model.

In this study, we use the multiplicative model to relate the precipitation estimates to the true value; however, without having the truth or making any assumptions about the distribution of the error, we estimate the RMSE of each estimate. Taking the logarithm of Eq. (1) results in

$$\ln(\mathbf{R}_i) = \alpha_i + \beta_i \ln(\mathbf{T}) + \boldsymbol{\epsilon}_i, \tag{2}$$

in which $\alpha_i = \ln(a_i)$ is the offset. Defining $\mathbf{r}_i = \ln(\mathbf{R}_i)$ and $\mathbf{t} = \ln(\mathbf{T})$, the equation is simplified to

$$\mathbf{r}_i = \alpha_i + \beta_i \mathbf{t} + \boldsymbol{\epsilon}_i. \tag{3}$$

This linear equation makes it possible to apply TC to the precipitation data, assuming a multiplicative error model. Therefore, log-transformation of the precipitation estimates from all the products is performed in this study and then TC is applied. Assuming there are three collocated estimates of precipitation with zero mean residual errors ($E(\boldsymbol{\epsilon}_i) = 0$) that are uncorrelated with each other ($\mathrm{Cov}(\boldsymbol{\epsilon}_i, \boldsymbol{\epsilon}_j) = 0$) and with the true precipitation ($\mathrm{Cov}(\boldsymbol{\epsilon}_i, \mathbf{t}) = 0$), the RMSE of each product can be estimated using the following sets of equations (McColl et al., 2014):

$$\sigma^2_{r_1} = C_{11} - \frac{C_{12}C_{13}}{C_{23}} \tag{4}$$

$$\sigma^2_{r_2} = C_{22} - \frac{C_{12}C_{23}}{C_{13}} \tag{5}$$

$$\sigma^2_{r_3} = C_{33} - \frac{C_{13}C_{23}}{C_{12}}, \tag{6}$$

where C_{ij} is the (i, j)th element of the sample covariance matrix between the transformed triplets, and σ_{r_i} is the RMSE of the $\mathbf{r}_i$ product. Equations (4)–(6) estimate the mean square error of each product in logarithmic scale. In Sect. 4, the results of these estimates along with RMSE estimates of $\mathbf{R}_i$ products are presented.

Based on the ETC introduced by McColl et al. (2014), the correlation coefficient between the truth and each of the triplets is

$$\rho^2_{t,1} = \frac{C_{12}C_{13}}{C_{11}C_{23}} \tag{7}$$

$$\rho^2_{t,2} = \frac{C_{12}C_{23}}{C_{22}C_{13}} \tag{8}$$

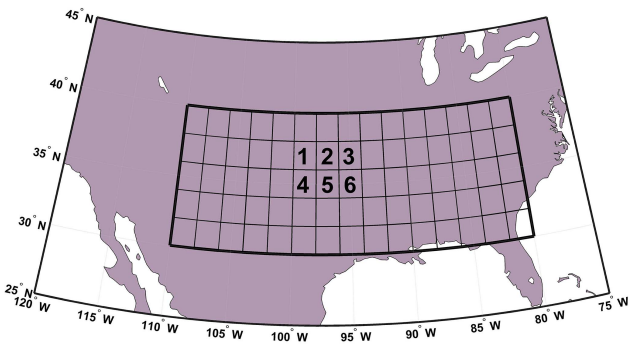

Figure 1. Study domain. The six numbered pixels are used in Sect. 5 for evaluation of TC assumptions in estimating RMSE.

$$\rho^2_{t,3} = \frac{C_{13}C_{23}}{C_{33}C_{12}}, \tag{9}$$

where $\rho^2_{t,i}$ is the correlation coefficient between the truth and product i in the logarithmic scale (i.e., between $\mathbf{t}$ and $\mathbf{r}_i$). In defining the sign of the $\rho_{t,i}$, it is assumed that the measurements are positively correlated with the truth to overcome sign ambiguity.

3 Study domain and data pre-processing

Figure 1 shows the analysis domain and the spatial grid used in this study. The study domain ranges from 30 to 40° N latitude and 110 to 80° W longitude. This region is selected to maximize the overlapping spatial coverage between the data sets that are used here. Major waterbodies (Great Lakes and the Gulf of Mexico) and strong terrain (i.e., Rocky Mountains) are excluded.

Precipitation estimates from five products NEXRAD-IV, TRMM 3B42RT, TRMM 3B42, GPI, and GPCP 1DD are evaluated. NEXRAD-IV is the national mosaicked precipitation estimates from the National Weather Service ground-based WSR-88D radar network (National Center for Environmental Prediction, 2005; Fulton et al., 1998). This product is based on merged gauge and radar estimates from 12 river forecast centers across the Continental United States (CONUS) that are mosaicked to a 4km grid over CONUS. The product is available through the National Center for Atmospheric Research (NCAR) Earth Observing Laboratory (EOL; Lin and Mitchell, 2005). Using nearest neighbor sampling, we map this product to a $0.05° \times 0.05°$ latitude–longitude grid. The original NEXRAD-IV (hereafter called NEXRAD) product is hourly accumulation in mm and is available from January 2002 to present.

TRMM 3B42RT is a multi-satellite precipitation estimate from the Tropical Rainfall Measuring Mission (TRMM) together with other low-earth-orbit microwave instruments (TRMM, 2015; Huffman et al., 2007). The precipitation estimates from several microwave instruments are calibrated

against the merged radar and radiometer precipitation products from TRMM, and then merged to produce a near-global 3 h precipitation product. The pixels with no microwave instrument observations are filled with measurements from IR instruments on board geostationary satellites that are calibrated using Passive Microwave (PMW) measurements. The TRMM 3B42RT is the real-time version of the product that does not have a gauge correction; however, the TRMM 3B42 is a gauge-corrected product, meaning that the monthly accumulation of estimates in each pixel are calibrated against GPCC gauge products to have similar monthly magnitudes. These two products are available on a $0.25^\circ \times 0.25^\circ$ latitude–longitude grid from January 1998 to present. We use the current V7 of them.

The GOES Precipitation Index (GPI) is a rainfall retrieval algorithm that only uses cloud-top temperatures from IR-based observations of geostationary satellites to estimate rain rate (Arkin and Meisner, 1987; Arkin and Janowiak, 2015). The main advantage of this product is that it only uses observations from geostationary satellites that are frequently available across the globe. However, the physics of the precipitation process is not considered in this retrieval algorithm. Therefore, the estimates are only useful in the tropics and warm-season extra-tropics in which most of the precipitation originates from deep convective cloud systems. This product contains daily precipitation rates on a $1^\circ \times 1^\circ$ spatial grid from October 1996 to present.

The Global Precipitation Climatology Project (GPCP) is a globally merged daily precipitation rate at $1^\circ \times 1^\circ$ spatial resolution from October 1996 to the present (Huffman et al., 2001, 2013). This is a merged estimate of precipitation from low-earth-orbit PMW instruments, the GOES IR-based observations, and surface rain gauge measurements. The merging approach utilizes the higher accuracy of the PMW observations to calibrate the more frequent GOES observations. In this study, V1.2 of the One-Degree Daily (1DD) product of GPCP is used.

The NEXRAD, TRMM 3B42, and TRMM 3B42RT data are upscaled to a $1^\circ \times 1^\circ$ spatial grid to be consistent with the spatial resolution of the GPI and GPCP 1DD data.

The time domain for this error estimation study is from January 2002 until April 2014. All the data products have a complete record within this time window which is more than 1 decade. Moreover, to generate temporally uncorrelated samples that do not have zero precipitation, the data from each product are temporally aggregated to biweekly values. Precipitation is a bounded variable and can only take values greater and equal to zero. If the precipitation estimate at a specific time and space is equal to zero; then, the error in that estimate can be from a limited set of numbers (basically any number greater than zero). Therefore, the error is dependent on the measurement (or equivalently the truth). As a result, if we have zero value in the precipitation measurement for all the triplets, the error of each of them is dependent on the measurement; and therefore, on each other. This dependence would violate the assumption that all errors are independent and identically distributed. The error dependence decreases as the measurement value moves away from zero. Among the aggregated data, there are a few percentage of samples that have zero biweekly precipitation accumulation which are removed from the analysis. The percentage of samples with zero value is less than 2% in most of the region other than eight pixels in the southwest of the region (the driest part of the domain) that have up to 8 % of the samples equal to zero. In the accumulation algorithm, any biweekly data with missing hourly or daily measurements are treated as missing values.

This data aggregation reduces the number of samples across the temporal domain of this study. TC analysis needs enough samples to be able to provide an accurate estimation of the error. Therefore, we combine the estimates from four neighboring $1^\circ \times 1^\circ$ pixels to form data points for the $2^\circ \times 2^\circ$ grids shown in Fig. 1. This means measurements taken over each of the four $1^\circ \times 1^\circ$ pixels inside the $2^\circ \times 2^\circ$ pixel are each treated to be measurements over the $2^\circ \times 2^\circ$ pixel, increasing the total number of samples for each $2^\circ \times 2^\circ$ pixel. Under the assumption that the estimated rainfall is statistically homogeneous over each $2^\circ \times 2^\circ$ pixel, we can trade off space and time in this way to increase the number of samples.

In the main analyses of the paper, the four products NEXRAD, TRMM 3B42RT, GPI, and GPCP 1DD are used. The TRMM 3B42 is used in Sect. 5 to show the impact of gauge correction on the estimated error characteristics. Figure 2 shows the climatology of precipitation derived from each of the four products. There is a good agreement between NEXRAD, TRMM 3B42RT, and GPCP 1DD estimates; however, GPI has a different climatological pattern across the domain. This difference is not unexpected. GPI's retrieval algorithm is very simple and only considers the cloud-top temperature; therefore, it is less accurate compared to the other three products that are either based on ground-based radar or have microwave estimates of precipitation combined with IR-based observations.

4 Results of TC analysis

In this section, we apply the multiplicative TC technique to the precipitation products introduced in Sect. 3 and present the estimated RMSE and correlation coefficients for each of the products. The four products are grouped to two triplets; Group 1 includes NEXRAD, TRMM 3B42RT, and GPI products, and Group 2 includes NEXRAD, TRMM 3B42RT, and GPCP 1DD. Similar results were obtained from other triplet combinations (these are not shown here).

Figures 3 and 4 show the RMSE of each $\mathbf{r}_i$ product in groups 1 and 2, respectively. These figures also show the number of data points (biweekly precipitation measurements) that are used in each pixel to do the TC estimate. Generally there are more than 1000 data points in each pixel. The

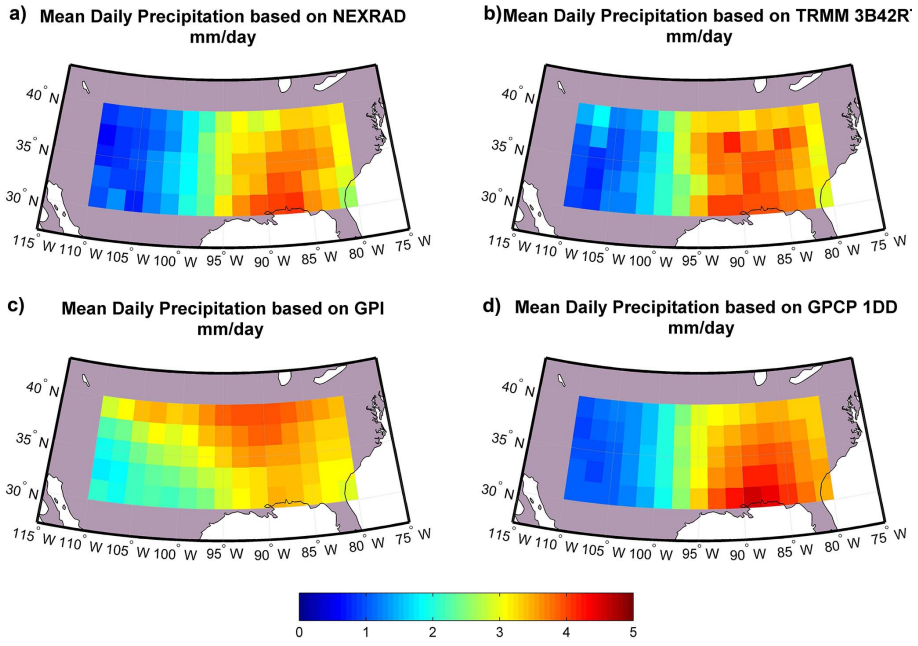

Figure 2. Climatology of precipitation across the study domain from each of the products.

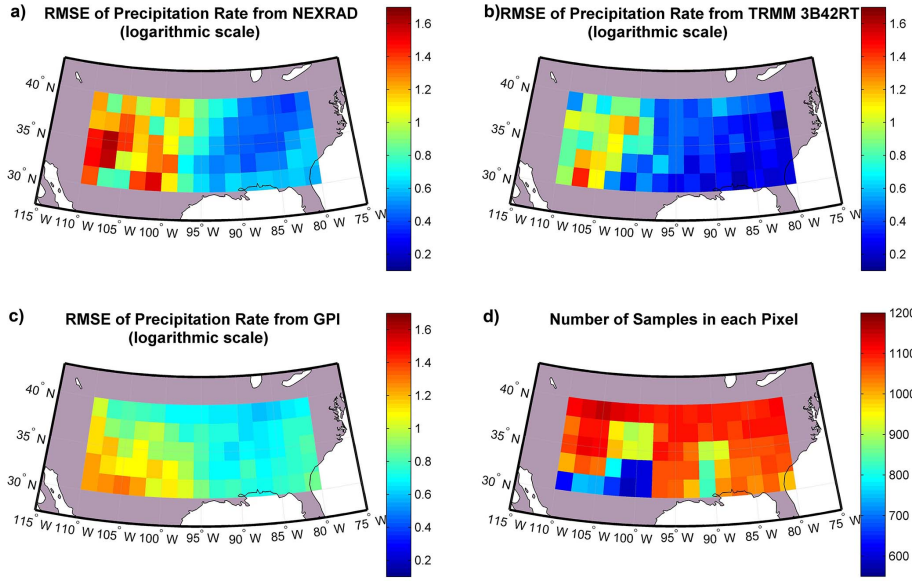

Figure 3. RMSE of the precipitation rate in logarithmic scale estimated from TC using triplets in group 1; **(a)** NEXRAD, **(b)** TRMM 3B42RT, **(c)** GPI. **(d)** shows the number of data points (biweekly measurements) in each pixel that are used for error estimation in TC analysis.

sharp decline in the number of data points in the pixels in the southwest of the study domain is due to the NEXRAD product, of which one of its radar systems was repeatedly inactive during 2002 and 2003.

The RMSE reported in these figures is based on bootstrap analysis. We run 1000 bootstrap simulations (i.e., sampling with replacement from the original data time series) and estimate the RMSE using Eqs. (4)–(6). The mean of these 1000 RMSE estimates is reported in Figs. 3 and 4. Additionally, the standard deviation of these bootstrap estimates is reported in Fig. S1 in the Supplement. The standard deviations of RMSE from the bootstrap simulations are 1 order of magnitude smaller than the RMSE estimate itself and the results are consistent between the two groups. GPI has a more uniform pattern for standard deviation of RMSE compared to NEXRAD, TRMM 3B42RT, and GPCP 1DD that have the east–west pattern. The standard deviation plots provide a range of confidence on the RMSE estimates from TC

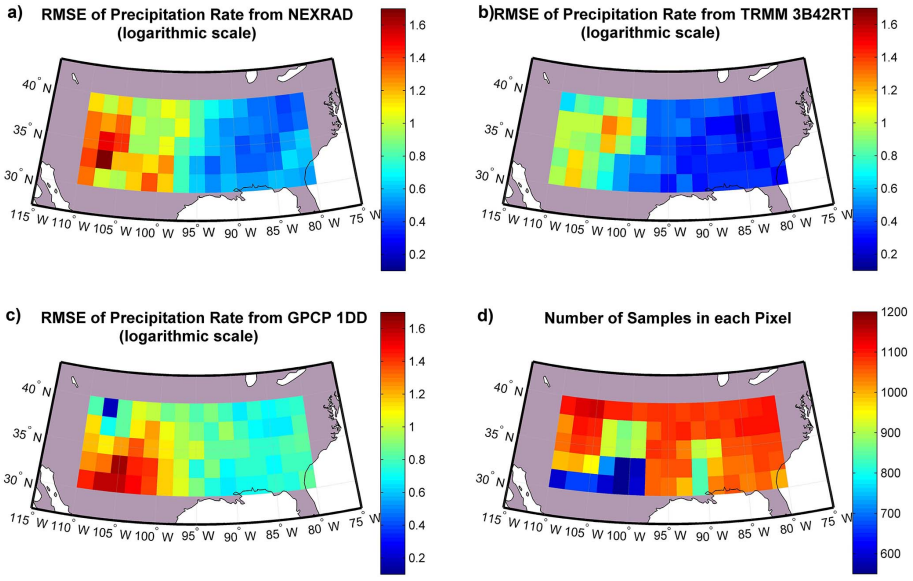

Figure 4. RMSE of the precipitation rate in logarithmic scale estimated from TC using triplets in group 2; **(a)** NEXRAD, **(b)** TRMM 3B42RT, **(c)** GPCP 1DD. **(d)** shows the number of data points (biweekly measurements) in each pixel that are used for error estimation in TC analysis.

analysis. Since the standard deviations are an order of magnitude smaller than the RMSE itself, the mean RMSE from the bootstrap simulations is a reasonable estimate of the RMSE.

The first observation and control check from Figs. 3 and 4 is that the RMSE estimates of precipitation from NEXRAD and TRMM 3B42RT in both of the groups are very similar. This shows that the TC analysis is robust and the results are not, in general, dependent on the choice of triplets. Moreover, the TRMM 3B42RT product has a lower RMSE in most of the region.

The RMSE estimates, shown in Figs. 3 and 4, are in logarithmic scale which is informative and useful if someone is assimilating the products in the logarithmic scale (equivalently using the $\mathbf{r}_i$ products). However, the RMSE estimates of $\mathbf{R}_i$ products in units of precipitation intensity (mm day^{-1} in this case) provide another perspective and might be simpler to interpret. Denoting μ_{R_i} as the mean of $\mathbf{R}_i$, expansion of Eq. (2) using Taylor series results in

$$\ln(\mathbf{R}_i) \approx \ln(\mu_{R_i}) + (\mathbf{R}_i - \mu_{R_i}) \frac{1}{\mu_{R_i}}. \quad (10)$$

Therefore,

$$\mathrm{Var}[\mathbf{r}_i] = \left(\frac{1}{\mu_{R_i}}\right)^2 \mathrm{Var}\left[(\mathbf{R}_i - \mu_{R_i})\right] \quad (11)$$

$$\sigma_{r_i}^2 = \left(\frac{1}{\mu_{R_i}}\right)^2 \sigma_{R_i}^2 \quad (12)$$

$$\sigma_{R_i} = \mu_{R_i} \sigma_{r_i}. \quad (13)$$

Equation (13) is used to report the RMSE of each of the precipitation product errors after carrying out the TC analysis on the log-transformed products. Figures 5 and 6 show the RMSE of precipitation products in each group in units of mm day.$^{-1}$ The standard deviations of these RMSE estimates are also presented in Fig. S2.

There is, again, consistency between the results of NEXRAD and TRMM 3B42RT in both groups. The RMSE of the TRMM 3B42RT product in both of the triplets and in majority of the pixels is small compared to the other two products, and it is also relatively small compared to the mean precipitation from climatology maps in Fig. 2. NEXRAD has relatively higher RMSE compared to TRMM 3B42RT, but is considerably smaller than GPCP 1DD or GPI.

Comparing the pattern of RMSE in NEXRAD, TRMM 3B42RT, and GPCP 1DD with the climatology maps (Fig. 2), it is clear that the RMSE in each product increases east to west, similar to the climatology. This means that in regions with higher mean precipitation rate, the RMSE is higher. This is consistent with other studies that have found that the mean error of precipitation estimates is proportional to the mean precipitation (Tian et al. (2013); Gebregiorgis and Hossain (2014); Tang et al. (2014); Alemohammad et al. (2014), among others).

A recent study by Prat and Nelson (2015) investigates the error of several precipitation products (ground-based radar and microwave instruments) over CONUS by assuming the gauge data as truth. They mainly characterize the bias in precipitation estimates and evaluate detection of precipitation events at different intensity thresholds and timescales. However, their results show a similar pattern in the error estimates; higher estimation errors for higher mean precipitation.

Figure 7 shows the estimated correlation coefficients between the underlying truth and each precipitation product in

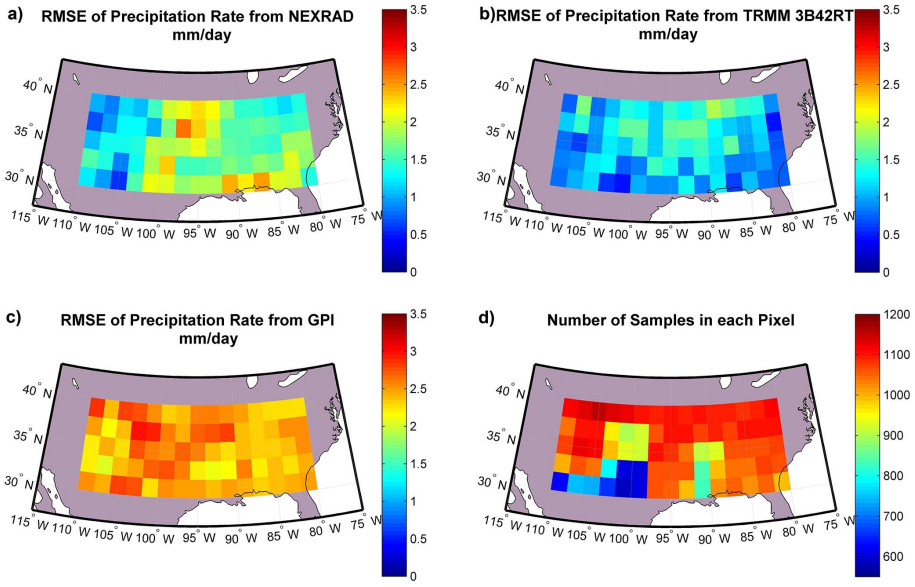

Figure 5. RMSE of the precipitation rate estimated from TC using triplets in group 1; **(a)** NEXRAD, **(b)** TRMM 3B42RT, **(c)** GPI. **(d)** shows the number of data points (biweekly measurements) in each pixel that are used for error estimation in TC analysis.

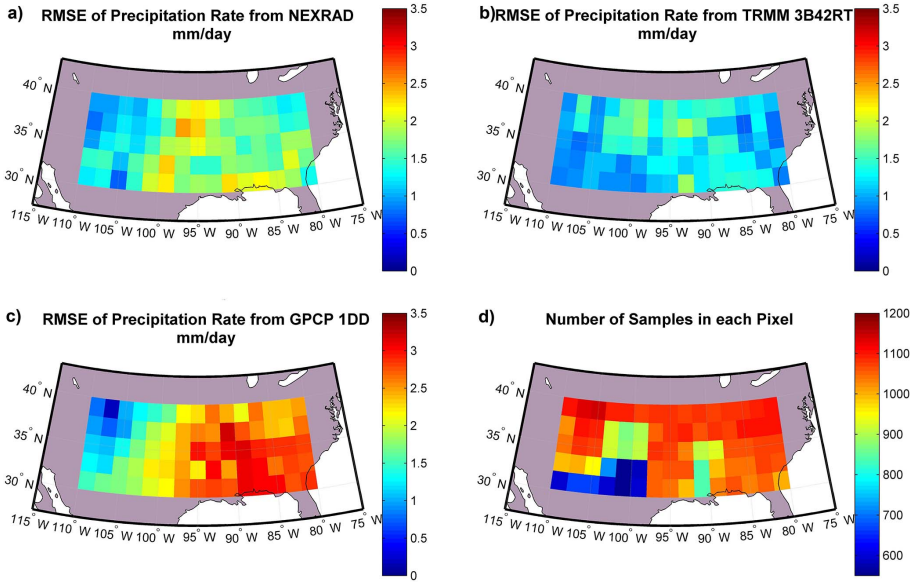

Figure 6. RMSE of the precipitation rate estimated from TC using triplets in group 2; **(a)** NEXRAD, **(b)** TRMM 3B42RT, **(c)** GPCP 1DD. **(d)** shows the number of data points (biweekly measurements) in each pixel that are used for error estimation in TC analysis.

the logarithmic scale. Similar to Figs. S1 and S2, each column shows the results of one of the triplet groups. Estimates of ρ^2 for TRMM 3B42RT and NEXRAD products from the two groups are very similar and this again shows the robustness of results from the TC technique. Among the products analyzed here, the TRMM 3B42RT product has the highest correlation coefficient with the truth in majority of the pixels, and NEXRAD is ranked second after TRMM 3B42RT. There is also a pattern that pixels toward the east of the region have higher correlation coefficients compared to the west of the region. GPCP 1DD has less correlation with the truth, and it has a similar east–west pattern. GPI exhibits very low correlation coefficients (~ 0.1) toward the west of the region.

The combined and quantitative analyses of the RMSE estimate and the correlation coefficients show that the TRMM 3B42RT product has the best performance among the four products considered here. The RMSE for TRMM 3B42RT has relatively less variation across the do-

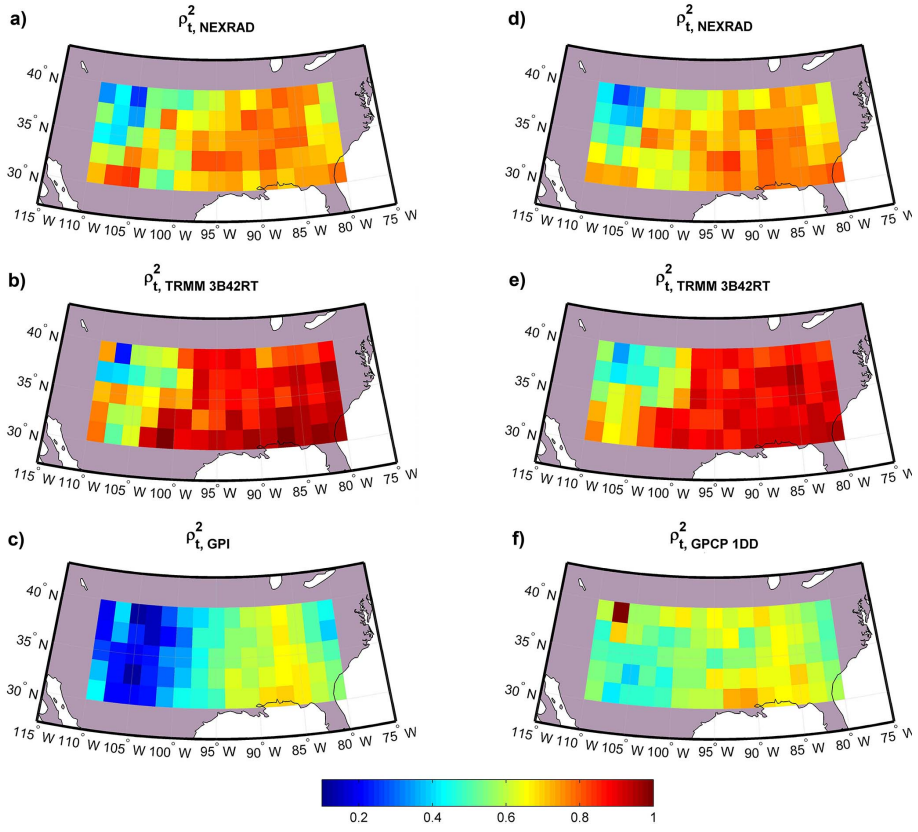

Figure 7. Correlation coefficient between the truth and each precipitation product. The left column shows the results for triplets in group 1, and the right column shows the results for triplets in group 2.

main. This means that the TRMM 3B42RT product has better performance in diverse climatic and geographical conditions. However, the correlation coefficients in TRMM 3B42RT decrease in the west side of the domain. This region is the coldest and snowiest part of the domain and it is covered with snow during the winter. The accuracy of microwave-based precipitation retrievals, which are the input measurements to the TRMM 3B42RT product, is affected by the snow on the ground. Some of the retrieval algorithms for these instruments cannot appropriately distinguish the snow on the ground from the falling precipitation. This phenomenon can contribute to the low correlation coefficient between the TRMM 3B42RT and the truth in the west part of the domain.

The NEXRAD product has a distinct error pattern. Both the RMSE and correlation coefficient of the NEXRAD estimates are small toward the west of the domain. However, comparing the error estimates from NEXRAD with the climatology values reveals that the errors are sometimes on the same order as the climatology toward the west of the domain. This is also revealed by the correlation coefficient values, which have a smaller value in the west side of the domain for NEXRAD. This pattern is consistent with the NEXRAD coverage maps provided by Maddox et al. (2002) that show the effect of terrain on radar beam blockage in mountainous regions of CONUS. Beam blockage is one of the sources of error in ground-based radar estimates of precipitation in mountainous regions.

The GPI and GPCP 1DD products are, in general, lower quality than TRMM 3B42RT and NEXRAD. They have higher RMSE and lower correlation coefficients with the truth. They both show the east–west pattern in the correlation coefficient; however, the GPI product has a sharper gradient and is poorly correlated with the truth toward the west of the study domain. Precipitation events in this region are mostly driven by frontal systems that generate clouds not necessarily well-correlated to precipitation; therefore, the GPI estimates that are solely based on cloud-top temperature are not well correlated with the truth. GPCP 1DD also uses IR-based observations of the clouds, but those are merged with microwave observations from low-earth-orbit satellites that are more accurate. Therefore, the resulting correlation coefficients are generally higher, especially in the west side of the study domain. If the analysis was limited to the RMSE estimates, GPI might be considered to be performing uniformly well across the entire domain. But with the correlation coefficients, we can clearly see the change in quality of GPI estimates across the domain.

5 Gauge analysis

In this section, we will review the assumptions that are embedded in TC estimates of RMSE and evaluate them using in situ gauge data. Gauge data are used a proxy for truth. As mentioned in Sect. 2, TC assumes zero correlation between errors of the triplets (the zero-error cross-covariance assumption) and between the errors and the truth (error orthogonality assumption). However, this assumption can be violated in many applications if the retrieval algorithms have similar error structures. Yilmaz and Crow (2014) investigated the assumptions of TC and introduced a decomposition of RMSE, derived from TC as following:

$$\sigma^2_{\mathrm{TC}_1} = \sigma^2_{\mathrm{TRE}_1} + \sigma^2_{\mathrm{LS}_1} + \sigma^2_{\mathrm{OE}_1} + \sigma^2_{\mathrm{XCE}_1}. \quad (14)$$

In this equation, $\sigma^2_{\mathrm{TC}_1}$ is the error variance of product 1 that is estimated by TC, and $\sigma^2_{\mathrm{TRE}_1}$ is the true error variance of product 1 that TC is aiming to estimate. $\sigma^2_{\mathrm{LS}_1}$ is the leaked portion of σ^2_{T} (the variance of the true data), $\sigma^2_{\mathrm{OE}_1}$ represents the bias term due to the violation of error orthogonality assumption, and $\sigma^2_{\mathrm{XCE}_1}$ is the bias term due to the violation of the zero-error cross-covariance assumption between different products. Note, $\sigma^2_{\mathrm{XCE}_1}$ is affected by the non-zero-error cross covariance between any pair of the products, and it is not only between product 1 and the gauge. Using similar notations as in Sect. 2, these four elements are defined as

$$\sigma^2_{\mathrm{TRE}_1} = \overline{\boldsymbol{\epsilon}_1\boldsymbol{\epsilon}_1} \quad (15)$$

$$\sigma^2_{\mathrm{LS}_1} = \left(\beta_1 - c_{3|1}\beta_3\right)\left(\beta_1 - c_{2|1}\beta_2\right)\sigma_t^2 \quad (16)$$

$$\sigma^2_{\mathrm{OE}_1} = \left(\beta_1 - c_{3|1}\beta_3\right)\left(\overline{\mathbf{t}\boldsymbol{\epsilon}_1} - c_{2|1}\overline{\mathbf{t}\boldsymbol{\epsilon}_2}\right) + \left(\beta_1 - c_{2|1}\beta_2\right)\left(\overline{\mathbf{t}\boldsymbol{\epsilon}_1} - c_{3|1}\overline{\mathbf{t}\boldsymbol{\epsilon}_3}\right) \quad (17)$$

$$\sigma^2_{\mathrm{XCE}_1} = -c_{2|1}\overline{\boldsymbol{\epsilon}_1\boldsymbol{\epsilon}_2} - c_{3|1}\overline{\boldsymbol{\epsilon}_1\boldsymbol{\epsilon}_3} + c_{3|1}c_{2|1}\overline{\boldsymbol{\epsilon}_2\boldsymbol{\epsilon}_3}, \quad (18)$$

in which $c_{i|j}$ is the scaling factor of product i assuming product j as the reference, and the overbar refers to temporal averaging. Equations (15)–(18) indicate the error decomposition for product 1 in the triplet. Similar equations can be derived for other products. Derivations of equations for these decomposition terms using the multiplicative error model are presented in Appendix A. For a detailed explanation on how to estimate different variables in these equations, the reader is referred to Sect. 2.c of Yilmaz and Crow (2014).

For this evaluation analysis, we need accurate ground-based observations in order to avoid errors due to differences in the spatial coverage between the gauges and the other products. The six pixels shown in Fig. 1 are selected for this evaluation since they have a dense network of rain gauges. These pixels are located in the state of Oklahoma and the gauge data are retrieved from the Oklahoma Mesonet network. This network provides quality-controlled daily precipitation estimates across the state of Oklahoma from an automatic and spatially dense set of rain gauges. We have located the gauges in each of the pixels; each pixel at every time contains at least 12 gauges and some of the pixels have up to 39 monitoring gauges. The daily data from the gauges in each pixel are averaged to estimate the true rain of the pixel and are then accumulated to biweekly values.

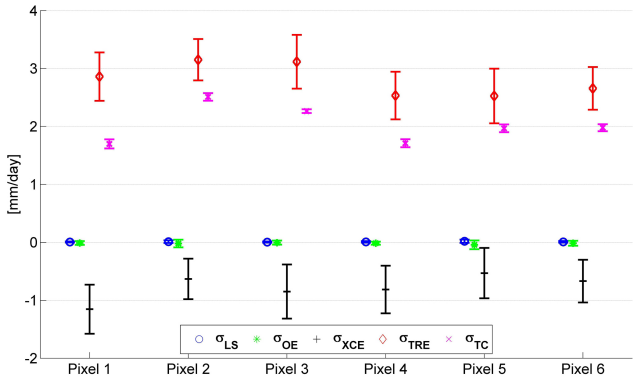

Figure 8. Decomposition of TC-based estimates of RMSE in the NEXRAD product across the six pixels shown in Fig. 1. Error bars show 1 standard deviation of the estimates from a bootstrap run with 100 samples.

It is understood that gauge data also have errors including representativeness error (they are point measurements unlike the other products that provide an average value over each pixel); however, as it is shown in Yilmaz and Crow (2014) (Appendix A) the representativeness error in the gauge measurements causes a positive bias in the TC-based RMSE estimates, while the cross-correlation between the errors of different products in each triplet causes a negative bias. Therefore, it is reasonable to assume gauge data to be an unbiased estimate of truth. Moreover, in this study the average of estimates from several gauges is used as the unbiased estimate of the truth. The representativeness error of the gauge estimates is basically interpreted as part of the total error variance in the gauge product. However, since the gauge estimates are unbiased estimates of the truth, it can be used a proxy to decompose the error variance estimates from the TC technique.

Figure 8 shows the results of error decomposition for the RMSE of the NEXRAD product. These estimates are based on another bootstrap simulation with 1000 samples, with corresponding 1 standard deviation confidence intervals. This figure shows that the bias caused by the leaked signal and error orthogonality assumption is almost zero in all of the cases. However, the zero-error cross-covariance assumption is causing significant underestimation in the RMSE estimated by TC. Therefore, the NEXRAD RMSE estimate from TC is a lower bound for the error. Figures S3–S5 show similar decomposition of the RMSE in TRMM 3B42RT,

GPCP 1DD, and GPI products across these pixels. These figures also confirm that the violation of the zero cross-covariance error leads to underestimation of the true RMSE by TC analysis. The noticeable difference between Figs. 8, S3, S4, and S5 is that in Fig. S5, which shows the error decomposition of GPI products, the contribution of error cross covariance to the total TC estimate is small, and in four of the pixels, it is almost zero. This is consistent with the fact that GPI has a completely different retrieval algorithm and is only based on cloud-top temperature measurements. Therefore, it has less correlation with other products. These results are consistent with the findings in Yilmaz and Crow (2014). Moreover, this analysis shows that similar to the soil moisture data, it is appropriate to assume that the errors of precipitation products are not correlated with the truth.

Here, we compare the ranking of the products based on the TC-derived errors and the ones based on the gauge analysis (σ_{TRE}). The goal of this comparison is to show how much the violation of the zero-error cross covariance impacts the RMSE estimates. In all of the six pixels that we conducted the gauge-based analysis, the TRMM 3B42RT and NEXRAD products are ranked first and second for the lowest error, based on the RMSE from TC, respectively. Moreover, based on the rankings in the gauge-based TC analysis (σ_{TRE} in Figs. 8, S3, S4, and S5) in five out of the six pixels, TRMM 3B42RT has the lowest error, and in four out of the six, NEXRAD has the best error after TRMM 3B42RT. However, GPCP 1DD and GPI rankings are only preserved on three out of the six pixels. Therefore, in general, we can make the conclusion that the relative rankings for the products with the lowest error remain almost the same, but it is hard to make any conclusion about the ranking of the other products. Nevertheless, this is based on only six pixels out of the 75 pixels across the whole domain. Therefore, it is not possible to extend this conclusion to the whole study. We can conclude from this comparison that the cross-correlation error can impact the performance ranking of the precipitation products, but the relative impact needs further analysis.

To further evaluate the impact of error cross covariance, we replace the TRMM 3B42RT product with the TRMM 3B42 product, and estimate the RMSEs in each triplet again. As it was mentioned in Sect. 3, the TRMM 3B42 product has a monthly gauge correction in its estimation algorithm. Our hypothesis is that this gauge dependence increases the error cross covariance between different products and will lead to lower RMSE estimates in NEXRAD, TRMM 3B42, and GPCP 1DD (these three have gauge correction in their algorithms) compared to the initial estimate using TRMM 3B42RT. We conducted this analysis and the resulting RMSE estimates from two triplets (NEXRAD, TRMM 3B42, GPI) and (NEXRAD, TRMM 3B42, GPCP 1DD) are presented in Figs. S6 and S7. Comparing Figs. 5 and 6 with Figs. S6 and S7, it is evident that the TC-derived error estimates of NEXRAD, TRMM 3B42, and GPCP 1DD are smaller when using the non real-time version of the TRMM 3B42 product. This further confirms that violation of the zero-error cross covariance causes a negative bias in the TC-based RMSE estimates.

6 Conclusions

This study presents, for the first time, error estimates of four precipitation products across a central part of the continental US using triple collocation (TC). A multiplicative error model is introduced to TC analysis that is a more realistic error model for precipitation. Furthermore, an extended version of TC is used with which not only the standard deviation of random errors in each product, but the correlation coefficient of each product with respect to an underlying truth are estimated. The results show that the TRMM 3B42RT product performs relatively better than the other three products. TRMM 3B42RT has the lowest RMSE across the domain, and the highest correlation coefficient with the underlying truth. Meanwhile, NEXRAD performs relatively poorly in the west side of the study domain that is probably caused by the terrain beam blockage. The performance of the GPCP 1DD and GPI products was lower than that of TRMM 3B42RT and NEXRAD. GPI has significantly lower performance in the west side of the study domain, that is likely caused by the simple retrieval algorithm used in this product. Meanwhile, GPI has a reasonably good correlation with the underlying truth in the east side of the domain.

In the second part of the paper, an evaluation of the assumptions built into TC is carried out using surface gauge data as a proxy for the truth across selective pixels. These pixels have a dense coverage of in situ gauges. The results of this evaluation reveal that the TC error estimates underestimate the true error in different products due to a violation of the assumption of the zero-error cross covariance. Moreover, replacing the TRMM 3B42RT with TRMM 3B42 revealed that the gauge correction in the TRMM 3B42 violates the zero- error cross-covariance assumption and leads to smaller RMSE estimates. However, the results of RMSE estimates from TC have a lot of potential to be incorporated into data assimilation and data-merging algorithms.

Triple collocation analysis has a lot of potential to be applied to various precipitation products at a wide range of spatial and temporal resolutions. This will provide a better understanding of the true error patterns in different products. Error quantification of precipitation products is a necessity if one aims to merge precipitation estimates from several instruments/models. However, care should be taken in choosing triplets that have zero- or small-error cross covariance. Otherwise, the error variances will be underestimated.

The multiplicative error model used in this study is shown to be an appropriate choice relative to the additive model. However, it would be beneficial to investigate more complex models that can take into account any higher order dependence of the estimate of the truth. A modification to this

study would be to include a gauge-only precipitation product. This would reduce the error cross covariance between the products, since the gauge measurement system is different from the remote-sensing instruments. Although gauge estimates have representativeness error, this error will be part of the total error in the gauge product resulting in higher RMSE values of gauge product. Furthermore, conducting TC analysis on precipitation data with different temporal resolution will provide valuable insight on the performance of different products at different temporal scales. However, this should be carried out with care, as precipitation errors at certain temporal resolutions are highly correlated and are not appropriate for TC analysis. The code for implementing multiplicative triple collocation in MATLAB is available at https://github.com/HamedAlemo.

Appendix A: Error decomposition

In this section, we derive Eqs. (15)–18 starting with the multiplicative error model in logarithmic scale:

$$\mathbf{r}_i = \alpha_i + \beta_i \mathbf{t} + \boldsymbol{\epsilon}_i . \tag{A1}$$

Without loss of generality, we assume $\mathbf{r}_i$ and $\mathbf{t}$ be the anomalies from a climatological mean; then, the model is simplified to

$$\mathbf{r}_i = \beta_i \mathbf{t} + \boldsymbol{\epsilon}_i . \tag{A2}$$

Choosing product r_1 as the reference, the scaling factors are defined as

$$c_{2|1} = \frac{\overline{\mathbf{r}_1 \mathbf{r}_3}}{\overline{\mathbf{r}_2 \mathbf{r}_3}} \tag{A3}$$

$$c_{3|1} = \frac{\overline{\mathbf{r}_1 \mathbf{r}_2}}{\overline{\mathbf{r}_3 \mathbf{r}_2}}. \tag{A4}$$

Therefore, the rescaled data sets are defined as: $\mathbf{r}_2^* = c_{2|1}\,\mathbf{r}_2$ and $\mathbf{r}_3^* = c_{3|1}\,\mathbf{r}_3$. Then, TC-based error variance of product 1 is defined as

$$\sigma^2_{\mathrm{TC}_1} = \overline{\left(\mathbf{r}_1 - \mathbf{r}_3^*\right)\left(\mathbf{r}_1 - \mathbf{r}_2^*\right)}. \tag{A5}$$

Inserting r_2^*, r_3^* and Eq. (A2) into Eq. (A5):

$$\sigma^2_{\mathrm{TC}_1} = \overline{\left[\left(\beta_1 - c_{3|1}\beta_3\right)\mathbf{t} + \left(\boldsymbol{\epsilon}_1 - c_{3|1}\boldsymbol{\epsilon}_3\right)\right]\left[\left(\beta_1 - c_{2|1}\beta_2\right)\mathbf{t} + \left(\boldsymbol{\epsilon}_1 - c_{2|1}\boldsymbol{\epsilon}_2\right)\right]} \tag{A6}$$

$$\begin{aligned}\sigma^2_{\mathrm{TC}_1} = {} & \left(\beta_1 - c_{3|1}\beta_3\right)\left(\beta_1 - c_{2|1}\beta_2\right)\sigma_t^2 \\ & + \left(\beta_1 - c_{3|1}\beta_3\right)\left(\overline{\mathbf{t}\boldsymbol{\epsilon}_1} - c_{2|1}\overline{\mathbf{t}\boldsymbol{\epsilon}_2}\right) \\ & + \left(\beta_1 - c_{2|1}\beta_2\right)\left(\overline{\mathbf{t}\boldsymbol{\epsilon}_1} - c_{3|1}\overline{\mathbf{t}\boldsymbol{\epsilon}_3}\right) \\ & + \left(\overline{\boldsymbol{\epsilon}_1\boldsymbol{\epsilon}_1} - c_{2|1}\overline{\boldsymbol{\epsilon}_1\boldsymbol{\epsilon}_2} - c_{3|1}\overline{\boldsymbol{\epsilon}_1\boldsymbol{\epsilon}_3} + c_{3|1}c_{2|1}\overline{\boldsymbol{\epsilon}_2\boldsymbol{\epsilon}_3}\right).\end{aligned} \tag{A7}$$

Rewriting Eq. (A7) as

$$\sigma^2_{\mathrm{TC}_1} = \sigma^2_{\mathrm{TRE}_1} + \sigma^2_{\mathrm{LS}_1} + \sigma^2_{\mathrm{OE}_1} + \sigma^2_{\mathrm{XCE}_1}, \tag{A8}$$

where:

$$\sigma^2_{\mathrm{TRE}_1} = \overline{\boldsymbol{\epsilon}_1\boldsymbol{\epsilon}_1} \tag{A9}$$

$$\sigma^2_{\mathrm{LS}_1} = \left(\beta_1 - c_{3|1}\beta_3\right)\left(\beta_1 - c_{2|1}\beta_2\right)\sigma_t^2 \tag{A10}$$

$$\begin{aligned}\sigma^2_{\mathrm{OE}_1} = {} & \left(\beta_1 - c_{3|1}\beta_3\right)\left(\overline{\mathbf{t}\boldsymbol{\epsilon}_1} - c_{2|1}\overline{\mathbf{t}\boldsymbol{\epsilon}_2}\right) \\ & + \left(\beta_1 - c_{2|1}\beta_2\right)\left(\overline{\mathbf{t}\boldsymbol{\epsilon}_1} - c_{3|1}\overline{\mathbf{t}\boldsymbol{\epsilon}_3}\right)\end{aligned} \tag{A11}$$

$$\sigma^2_{\mathrm{XCE}_1} = -c_{2|1}\overline{\boldsymbol{\epsilon}_1\boldsymbol{\epsilon}_2} - c_{3|1}\overline{\boldsymbol{\epsilon}_1\boldsymbol{\epsilon}_3} + c_{3|1}c_{2|1}\overline{\boldsymbol{\epsilon}_2\boldsymbol{\epsilon}_3}. \tag{A12}$$

Equations (A9)–(A12) are the same as Eqs. (15)–(18) that are used to decompose the RMSE estimates of TC analysis.

The Supplement related to this article is available online at doi:10.5194/hess-19-3489-2015-supplement.

Acknowledgements. The authors wish to thank Wade Crow and another anonymous reviewer for their constructive feedback that led to improvements in this paper. The authors also thank all the producers and distributors of the data used in this study. The TRMM 3B42 and TRMM 3B42RT data used in this study were acquired as part of the NASA Earth-Sun System Division and archived and distributed by the Goddard Earth Sciences (GES) Data and Information Services Center (DISC). The GPCP 1DD data were provided by the NASA/Goddard Space Flight Center's Mesoscale Atmospheric Processes Laboratory, which develops and computes the 1DD as a contribution to the GEWEX Global Precipitation Climatology Project. The GPI data are produced by science investigators, Drs. Phillip Arkin and John Janowiak of the Climate Analysis Center, NOAA, Washington, D.C., and distributed by the Distributed Active Archive Center (Code 610.2) at the Goddard Space Flight Center, Greenbelt, MD, 20771. The Oklahoma Mesonet data are provided courtesy of the Oklahoma Mesonet, a cooperative venture between Oklahoma State University and The University of Oklahoma and supported by the taxpayers of Oklahoma.

Edited by: E. Morin

References

Alemohammad, S. H., Entekhabi, D., and McLaughlin, D. B.: Evaluation of Long-Term SSM/I-Based Precipitation Records over Land, J. Hydrometeorol., 15, 2012–2029, doi:10.1175/JHM-D-13-0171.1, 2014.

Alemohammad, S. H., McLaughlin, D. B., and Entekhabi, D.: Quantifying Precipitation Uncertainty for Land Data Assimilation Applications, Mon. Weather Rev., 143, 3276–3299, doi:10.1175/MWR-D-14-00337.1, 2015.

Anagnostou, E., Maggioni, V., Nikolopoulos, E., Meskele, T., Hossain, F., and Papadopoulos, A.: Benchmarking High-Resolution Global Satellite Rainfall Products to Radar and Rain-Gauge Rainfall Estimates, IEEE T. Geosci. Remote, 48, 1667–1683, doi:10.1109/TGRS.2009.2034736, 2010.

Anderson, W. B., Zaitchik, B. F., Hain, C. R., Anderson, M. C., Yilmaz, M. T., Mecikalski, J., and Schultz, L.: Towards an integrated soil moisture drought monitor for East Africa, Hydrol. Earth Syst. Sci., 16, 2893–2913, doi:10.5194/hess-16-2893-2012, 2012.

Arkin, P. and Janowiak, J.: Global Precipitation Index (GPI), Goddard Space Flight Center Distributed Active Archive Center (GSFC DAAC), http://disc.sci.gsfc.nasa.gov/precipitation/data-holdings/access/data_access_nonjs.shtml, last access: August 2015.

Arkin, P. A. and Meisner, B. N.: The Relationship between Large-Scale Convective Rainfall and Cold Cloud over the Western Hemisphere during 1982–84, Mon. Weather Rev., 115, 51–74, doi:10.1175/1520-0493(1987)115<0051:TRBLSC>2.0.CO;2, 1987.

Chen, S., Kirstetter, P. E., Hong, Y., Gourley, J. J., Tian, Y. D., Qi, Y. C., Cao, Q., Zhang, J., Howard, K., Hu, J. J., and Xue, X. W.: Evaluation of Spatial Errors of Precipitation Rates and Types from TRMM Spaceborne Radar over the Southern CONUS, J. Hydrometeorol., 14, 1884–1896, doi:10.1175/JHM-D-13-027.1, 2013.

Ciach, G. J., Krajewski, W. F., and Villarini, G.: Product-Error-Driven Uncertainty Model for Probabilistic Quantitative Precipitation Estimation with NEXRAD Data, J. Hydrometeorol., 8, 1325–1347, doi:10.1175/2007JHM814.1, 2007.

Cimini, D., Pierdicca, N., Pichelli, E., Ferretti, R., Mattioli, V., Bonafoni, S., Montopoli, M., and Perissin, D.: On the accuracy of integrated water vapor observations and the potential for mitigating electromagnetic path delay error in InSAR, Atmos. Meas. Tech., 5, 1015–1030, doi:10.5194/amt-5-1015-2012, 2012.

D'Odorico, P., Gonsamo, A., Pinty, B., Gobron, N., Coops, N., Mendez, E., and Schaepman, M. E.: Intercomparison of fraction of absorbed photosynthetically active radiation products derived from satellite data over Europe, Remote Sens. Environ., 142, 141–154, doi:10.1016/j.rse.2013.12.005, 2014.

Dorigo, W. A., Scipal, K., Parinussa, R. M., Liu, Y. Y., Wagner, W., de Jeu, R. A. M., and Naeimi, V.: Error characterisation of global active and passive microwave soil moisture datasets, Hydrol. Earth Syst. Sci., 14, 2605–2616, doi:10.5194/hess-14-2605-2010, 2010.

Draper, C., Reichle, R., de Jeu, R., Naeimi, V., Parinussa, R., and Wagner, W.: Estimating root mean square errors in remotely sensed soil moisture over continental scale domains, Remote Sens. Environ., 137, 288–298, doi:10.1016/j.rse.2013.06.013, 2013.

Ebert, E. E., Janowiak, J. E., and Kidd, C.: Comparison of Near-Real-Time Precipitation Estimates from Satellite Observations and Numerical Models, B. Am. Meteorol. Soc., 88, 47–64, doi:10.1175/BAMS-88-1-47, 2007.

Fang, H., Wei, S., Jiang, C., and Scipal, K.: Theoretical uncertainty analysis of global MODIS, CYCLOPES, and {GLOBCARBON} {LAI} products using a triple collocation method, Remote Sens. Environ., 124, 610–621, doi:10.1016/j.rse.2012.06.013, 2012.

Fulton, R. A., Breidenbach, J. P., Seo, D.-J., Miller, D. A., and O,Bannon, T.: The WSR-88D Rainfall Algorithm, Weather Forecast., 13, 377–395, doi:10.1175/1520-0434(1998)013<0377:TWRA>2.0.CO;2, 1998.

Gebregiorgis, A. and Hossain, F.: Estimation of Satellite Rainfall Error Variance Using Readily Available Geophysical Features, IEEE T. Geosci. Remote, 52, 288–304, doi:10.1109/TGRS.2013.2238636, 2014.

Gebregiorgis, A. S. and Hossain, F.: How well can we estimate error variance of satellite precipitation data around the world?, Atmos. Res., 154, 39–59, doi:10.1016/j.atmosres.2014.11.005, 2015.

Habib, E., Haile, A. T., Tian, Y., and Joyce, R. J.: Evaluation of the High-Resolution CMORPH Satellite Rainfall Product Using Dense Rain Gauge Observations and Radar-Based Estimates, J. Hydrometeorol., 13, 1784–1798, doi:10.1175/JHM-D-12-017.1, 2012.

Hossain, F. and Anagnostou, E. N.: A Two-Dimensional Satellite Rainfall Error Model, IEEE T. Geosci. Remote, 44, 1511–1522, doi:10.1109/TGRS.2005.863866, 2006.

Hou, A. Y., Kakar, R. K., Neeck, S., Azarbarzin, A. A., Kummerow, C. D., Kojima, M., Oki, R., Nakamura, K., and Iguchi, T.: The Global Precipitation Measurement Mission, B. Am. Meteorol. Soc., 95, 701–722, doi:10.1175/BAMS-D-13-00164.1, 2013.

Huffman, G. J., Adler, R. F., Morrissey, M. M., Bolvin, D. T., Curtis, S., Joyce, R., McGavock, B., and Susskind, J.: Global Precipitation at One-Degree Daily Resolution from Multisatellite Observations, J. Hydrometeorol., 2, 36–50, doi:10.1175/1525-7541(2001)002<0036:GPAODD>2.0.CO;2, 2001.

Huffman, G. J., Bolvin, D. T., Nelkin, E. J., Wolff, D. B., Adler, R. F., Gu, G., Hong, Y., Bowman, K. P., and Stocker, E. F.: The TRMM Multisatellite Precipitation Analysis (TMPA): Quasi-Global, Multiyear, Combined-Sensor Precipitation Estimates at Fine Scales, J. Hydrometeorol., 8, 38–55, doi:10.1175/JHM560.1, 2007.

Huffman, G. J., Adler, R. F., Morrissey, M. M., Bolvin, D. T., Curtis, S., Joyce, R., McGavock, B., and Susskind, J.: GPCP 1-Degree Daily Combination (Version 1.2), Goddard Space Flight Center's Mesoscale Atmospheric Processes Laboratory, http://precip.gsfc.nasa.gov/gpcp_daily_comb.html (last access: 10 January 2015), 2013.

Janssen, P. A. E. M., Abdalla, S., Hersbach, H., and Bidlot, J.-R.: Error Estimation of Buoy, Satellite, and Model Wave Height Data, J. Atmos. Ocean. Tech., 24, 1665–1677, doi:10.1175/JTECH2069.1, 2007.

Kirstetter, P.-E., Hong, Y., Gourley, J. J., Schwaller, M., Petersen, W., and Zhang, J.: Comparison of TRMM 2A25 Products, Version 6 and Version 7, with NOAA/NSSL Ground Radar-Based National Mosaic QPE, J. Hydrometeorol., 14, 661–669, doi:10.1175/JHM-D-12-030.1, 2012.

Kirstetter, P.-E., Viltard, N., and Gosset, M.: An error model for instantaneous satellite rainfall estimates: evaluation of BRAIN-TMI over West Africa, Q. J. Roy. Meteorol. Soc., 139, 894–911, doi:10.1002/qj.1964, 2013.

Krajewski, W. F., Ciach, G. J., McCollum, J. R., and Bacotiu, C.: Initial Validation of the Global Precipitation Climatology Project Monthly Rainfall over the United States, J. Appl. Meteorol., 39, 1071–1086, doi:10.1175/1520-0450(2000)039<1071:IVOTGP>2.0.CO;2, 2000.

Lin, Y. and Mitchell, K. E.: The NCEP Stage II/IV hourly precipitation analyses: development and applications, in: 19th Conf. on Hydrology, Paper 1.2, American Meteorological Society, San Diego, CA, http://www.emc.ncep.noaa.gov/mmb/ylin/pcpanl/refs/stage2-4.19hydro.pdf (last access: 10 January 2015), 2005.

Maddox, R. A., Zhang, J., Gourley, J. J., and Howard, K. W.: Weather Radar Coverage over the Contiguous United States, Weather Forecast., 17, 927–934, doi:10.1175/1520-0434(2002)017<0927:WRCOTC>2.0.CO;2, 2002.

Maggioni, V., Sapiano, M. R. P., Adler, R. F., Tian, Y., and Huffman, G. J.: An Error Model for Uncertainty Quantification in High-Time-Resolution Precipitation Products, J. Hydrometeorol., 15, 1274–1292, doi:10.1175/JHM-D-13-0112.1, 2014.

McColl, K. A., Vogelzang, J., Konings, A. G., Entekhabi, D., Piles, M., and Stoffelen, A.: Extended triple collocation: Estimating errors and correlation coefficients with respect to an unknown target, Geophys. Res. Lett., 41, 6229–6236, doi:10.1002/2014GL061322, 2014.

McCollum, J. R., Krajewski, W. F., Ferraro, R. R., and Ba, M. B.: Evaluation of Biases of Satellite Rainfall Estimation Algorithms over the Continental United States, J. Appl. Meteorol., 41, 1065–1080, doi:10.1175/1520-0450(2002)041<1065:EOBOSR>2.0.CO;2, 2002.

Miralles, D. G., Crow, W. T., and Cosh, M. H.: Estimating Spatial Sampling Errors in Coarse-Scale Soil Moisture Estimates Derived from Point-Scale Observations, J. Hydrometeorol., 11, 1423–1429, doi:10.1175/2010JHM1285.1, 2010.

National Center for Environmental Prediction: Precipitation NCEP/EMC 4KM Gridded Data (GRIB) Stage IV Data, National Center for Atmospheric Research, Earth Observing Laboratory, http://data.eol.ucar.edu/codiac/dss/id=21.093 (last access: 10 January 2015), 2005.

Parinussa, R. M., Holmes, T. R. H., Yilmaz, M. T., and Crow, W. T.: The impact of land surface temperature on soil moisture anomaly detection from passive microwave observations, Hydrol. Earth Syst. Sci., 15, 3135–3151, doi:10.5194/hess-15-3135-2011, 2011.

Portabella, M. and Stoffelen, A.: On Scatterometer Ocean Stress, J. Atmos. Ocean. Tech., 26, 368–382, doi:10.1175/2008JTECHO578.1, 2009.

Prat, O. P. and Nelson, B. R.: Evaluation of precipitation estimates over CONUS derived from satellite, radar, and rain gauge data sets at daily to annual scales (2002–2012), Hydrol. Earth Syst. Sci., 19, 2037–2056, doi:10.5194/hess-19-2037-2015, 2015.

Ratheesh, S., Mankad, B., Basu, S., Kumar, R., and Sharma, R.: Assessment of Satellite-Derived Sea Surface Salinity in the Indian Ocean, IEEE Geosci. Remote Sens. Lett., , 10, 428–431, doi:10.1109/LGRS.2012.2207943, 2013.

Roebeling, R. A., Wolters, E. L. A., Meirink, J. F., and Leijnse, H.: Triple Collocation of Summer Precipitation Retrievals from SEVIRI over Europe with Gridded Rain Gauge and Weather Radar Data, J. Hydrometeorol., 13, 1552–1566, doi:10.1175/JHM-D-11-089.1, 2012.

Salio, P., Hobouchian, M. P., Skabar, Y. G., and Vila, D.: Evaluation of High-Resolution Satellite Precipitation Estimates over Southern South America using a Dense Rain Gauge Network, Atmos. Res., 163, 146–161, doi:10.1016/j.atmosres.2014.11.017, 2015.

Sapiano, M. R. P. and Arkin, P. A.: An Intercomparison and Validation of High-Resolution Satellite Precipitation Estimates with 3-Hourly Gauge Data, J. Hydrometeorol., 10, 149–166, doi:10.1175/2008JHM1052.1, 2009.

Scott, K., Buehner, M., and Carrieres, T.: An Assessment of Sea-Ice Thickness Along the Labrador Coast From AMSR-E and MODIS Data for Operational Data Assimilation, IEEE T. Geosci. Remote, 52, 2726–2737, doi:10.1109/TGRS.2013.2265091, 2014.

Seyyedi, H.: Performance Assessment of Satellite Rainfall Products for Hydrologic Modeling, PhD thesis, University of Connecticut, http://digitalcommons.uconn.edu/dissertations/335 (last access: 10 January 2015), 2014.

Stampoulis, D. and Anagnostou, E. N.: Evaluation of Global Satellite Rainfall Products over Continental Europe, J. Hydrometeorol., 13, 588–603, doi:10.1175/JHM-D-11-086.1, 2012.

Stoffelen, A.: Toward the true near-surface wind speed: Error modeling and calibration using triple collocation, J. Geophys. Res.-Oceans, 103, 7755–7766, doi:10.1029/97JC03180, 1998.

Su, C.-H., Ryu, D., Crow, W. T., and Western, A. W.: Beyond triple collocation: Applications to soil moisture

monitoring, J. Geophys. Res.-Atmos., 119, 6419–6439, doi:10.1002/2013JD021043, 2014.

Su, F., Hong, Y., and Lettenmaier, D. P.: Evaluation of TRMM Multisatellite Precipitation Analysis (TMPA) and Its Utility in Hydrologic Prediction in the La Plata Basin, J. Hydrometeorol., 9, 622–640, doi:10.1175/2007JHM944.1, 2008.

Tang, L., Tian, Y., and Lin, X.: Validation of precipitation retrievals over land from satellite-based passive microwave sensors, J. Geophys. Res.-Atmospheres, 119, 4546–4567, doi:10.1002/2013JD020933, 2014.

Thao, S., Eymard, L., Obligis, E., and Picard, B.: Trend and Variability of the Atmospheric Water Vapor: A Mean Sea Level Issue, J. Atmos. Ocean. Tech., 31, 1881–1901, doi:10.1175/JTECH-D-13-00157.1, 2014.

Tian, Y., Peters-Lidard, C. D., Eylander, J. B., Joyce, R. J., Huffman, G. J., Adler, R. F., Hsu, K.-l., Turk, F. J., Garcia, M., and Zeng, J.: Component analysis of errors in satellite-based precipitation estimates, J. Geophys. Res.-Atmos., 114, D24101, doi:10.1029/2009JD011949, 2009.

Tian, Y., Huffman, G. J., Adler, R. F., Tang, L., Sapiano, M., Maggioni, V., and Wu, H.: Modeling errors in daily precipitation measurements: Additive or multiplicative?, Geophys. Res. Lett., 40, 2060–2065, doi:10.1002/grl.50320, 2013.

TRMM – Tropical Rainfall Measurement Mission Project (): TRMM 3-Hourly 0.25 deg. TRMM and Others Rainfall Estimate Data, version 7, Goddard Space Flight Center Distributed Active Archive Center (GSFC DAAC), http://disc.sci.gsfc.nasa.gov/datacollection/TRMM_3B42_V7.html, last access: 15 May 2015.

van Dijk, A. I. J. M., Renzullo, L. J., Wada, Y., and Tregoning, P.: A global water cycle reanalysis (2003–2012) merging satellite gravimetry and altimetry observations with a hydrological multi-model ensemble, Hydrol. Earth Syst. Sci., 18, 2955–2973, doi:10.5194/hess-18-2955-2014, 2014.

Vila, D. A., de Goncalves, L. G. G., Toll, D. L., and Rozante, J. R.: Statistical Evaluation of Combined Daily Gauge Observations and Rainfall Satellite Estimates over Continental South America, J. Hydrometeorol., 10, 533–543, doi:10.1175/2008JHM1048.1, 2009.

Villarini, G., Krajewski, W. F., Ciach, G. J., and Zimmerman, D. L.: Product-error-driven generator of probable rainfall conditioned on WSR-88D precipitation estimates, Water Resour. Res., 45, W01404, doi:10.1029/2008WR006946, 2009.

Yilmaz, M. T. and Crow, W. T.: Evaluation of Assumptions in Soil Moisture Triple Collocation Analysis, J. Hydrometeorol., 15, 1293–1302, doi:10.1175/JHM-D-13-0158.1, 2014.